AIP Proceedings

Doping Nanocrystals and the Role of Quantum Confinement

Tzu-Liang Chan, Murilo L. Tiago, and James R. Chelikowsky

Citation: AIP Conference Proceedings **931**, 555 (2007); doi: 10.1063/1.2799436
View online: http://dx.doi.org/10.1063/1.2799436
View Table of Contents: http://scitation.aip.org/content/aip/proceeding/aipcp/931?ver=pdfcov
Published by the AIP Publishing

Articles you may be interested in

A first-principles study of the electronic and structural properties of Sb and F doped SnO2 nanocrystals
J. Chem. Phys. **142**, 044704 (2015); 10.1063/1.4906150

Electronic structures and magnetic stabilities of 2D Mn-doped GaAs nanosheets: The role of long-range exchange interactions and doping strategies
J. Appl. Phys. **116**, 083912 (2014); 10.1063/1.4894395

First-principles theoretical analysis of transition-metal doping of ZnSe quantum dots
J. Appl. Phys. **112**, 024301 (2012); 10.1063/1.4734841

Adsorption of hydrogen on boron-doped graphene: A first-principles prediction
J. Appl. Phys. **105**, 014309 (2009); 10.1063/1.3056380

Quantum confinement in germanium nanocrystals
Appl. Phys. Lett. **77**, 1182 (2000); 10.1063/1.1289659

This article is copyrighted as indicated in the article. Reuse of AIP content is subject to the terms at: http://scitation.aip.org/termsconditions. Downloaded to IP: 128.83.205.78 On: Fri, 20 Mar 2015 15:45:07

Doping Nanocrystals and the Role of Quantum Confinement

Tzu-Liang Chan*, Murilo L. Tiago* and James R. Chelikowsky†

*Center for Computational Materials, Institute of Computational Engineering and Sciences, University of Texas, Austin, TX 78712 USA

†Center for Computational Materials, Institute of Computational Engineering and Sciences, Departments of Physics and Chemical Engineering, University of Texas, Austin, TX 78712 USA

Abstract. Recent progress in developing algorithms for solving the electronic structure problem for nanostructures is illustrated. Key ingredients in this approach include pseudopotentials implemented on a real space grid and the use of density functional theory. This procedure allows one to predict electronic properties for many materials across the nano-regime, *i.e.*, from atoms to nanocrystals of sufficient size to replicate bulk properties. We will illustrate this method for doping silicon nanocrystals with phosphorous.

Keywords: Nanostructures, doping, computational methods, algorithms, pseudopotentials, nanocrystals, nanowires

INTRODUCTION

One of the most significant goals in materials physics is the development of new algorithms and physical concepts for describing matter at all length scales, especially at the nano-scale. This goal has assumed more significance in past years owing to interest in the role of quantum confinement, *i.e.*, the physical localization of materials phenomena at the nano-scale [1]. Quantum confinement offers one opportunity to alter properties of matter without changing the chemical composition. For example, quantum confinement in CdSe nanocrystals can be used to tune the optical gap across the visible spectrum [2] or Si nanocrystals can be made optically active at small length scales [3, 4].

Predicting the role of quantum confinement and the properties of nanostructures is a difficult task owing to the complexity of such systems, which often contain thousands of atoms with little symmetry. This said, notable progress has been accomplished by implementing new computational methods. Here we will outline the nature of these methods and apply them to complex systems such as nanocrystals and nanowires.

COMPUTATIONAL METHODS

The spatial and energetic distributions of electrons can be described by a solution of the Kohn-Sham equation [5]:

$$\left(\frac{-\hbar^2\nabla^2}{2m} + V_{ion}^p + V_H + V_{xc} \right) \psi_n = E_n \psi_n \qquad (1)$$

where V_{ion}^p is an ionic pseudopotential [6], V_H is the Hartree or Coulomb potential, and V_{xc} is the exchange-correlation potential. The Hartree and exchange-correlation potentials can be determined from the electronic charge density. The density is given by

$$\rho(\vec{r}) = e \sum_{n,occup} |\psi_n(\vec{r})|^2 \qquad (2)$$

The summation is over all occupied states. The Hartree potential is then determined by

$$\nabla^2 V_H(\vec{r}) = -4\pi e \rho(\vec{r}) \qquad (3)$$

This term can be interpreted as the electrostatic interaction of an electron with the charge density of the system.

The exchange-correlation potential is more problematic. This potential can be evaluated using a *local density approximation*. The central tenet of this approximation is that the total exchange-correlation energy may be written as a universal functional of the density:

$$E_{xc}[\rho] = \int \rho(\vec{r})\ \varepsilon_{xc}[\rho(\vec{r})]\ d^3r \qquad (4)$$

where ε_{xc} is the exchange-correlation energy density. E_{xc} and ε_{xc} are to be interpreted as depending solely on the charge density. The exchange-correlation potential, V_{xc}, is then obtained as $V_{xc} = \delta E_{xc}[\rho]/\delta\rho$.

It is not difficult to solve the Kohn-Sham equation (Eq. 1) for an atom. The atomic charge density can be taken to be spherically symmetric. Thus, the Kohn-Sham problem reduces to solving a one-dimensional problem. The Hartree and exchange-correlation potentials can be iterated to form a self-consistent field. This atomic solution provides the input to construct a pseudopotential representing the effect of the core electrons and nucleus. This "ion core" pseudopotential, V_{ion}^p, can be transferred to other systems such as molecules and quantum dots [6].

CP931, *Frontiers of Characterization and Metrology for Nanoelectronics*,
edited by D. G. Seiler, A. C. Diebold, R. McDonald, C. M. Garner, D. Herr, R. P. Khosla, and E. M. Secula
© 2007 American Institute of Physics 978-0-7354-0441-0/07/$23.00

This article is copyrighted as indicated in the article. Reuse of AIP content is subject to the terms at: http://scitation.aip.org/termsconditions. Downloaded to IP: 128.83.205.78 On: Fri, 20 Mar 2015 15:45:07

The Kohn-Sham equations represent a nonlinear, self-consistent eigenvalue problem. Typically, a solution is obtained by first approximating the Hartree and exchange-correlation potentials using a superposition of atomic charge densities. The Kohn-Sham equation is then solved using these approximate potentials. From the solution, new wave functions and charge densities are obtained and used to construct updated Hartree and exchange-correlation potentials. The process is repeated until the "input" and "output" potentials agree and a self-consistent solution is realized. At this point, the total electronic energy can be computed along with a variety of other electronic properties [6].

Once the Kohn-Sham equation is solved, the total electronic energy, E_T, of the system can be evaluated from

$$E_T = \sum_{n,occup} E_n - \frac{1}{2}\int V_H(\vec{r})\rho(\vec{r})\, d^3r + \int \rho(\vec{r})\left[\varepsilon_{xc}(\rho(\vec{r})) - V_{xc}(\rho(\vec{r}))\right] d^3r \qquad (5)$$

where the energy eigenvalues are given by E_n.

The structure energy can be obtained by adding the ion core electrostatic terms [6]. The forces can be obtained by taking the derivative of the energy with respect to position.

The Kohn-Sham equation as cast in Eq. 1 can be solved using a variety of techniques. Often the wave functions can be expanded in a basis such as plane waves or gaussians and the resulting secular equations can be solved using standard diagonalization packages such as those found in VASP [7].

Here we focus on a different approach. We solve the Kohn-Sham equation without resort to an explicit basis [8, 9, 10, 11, 12]. We solve for the wave functions on the grid with a fixed domain, which encompasses the physical system of interest. The grid need not be uniform, but it greatly simplifies the problem if it is. The wave functions outside of the domain are required to vanish for confined systems or assume periodic boundary conditions for systems with translational symmetry. In contrast to methods employing an explicit basis, such boundary conditions are easily incorporated. In particular, real space methods do not require the use of supercells for localized systems. As such, charged systems can easily be examined without considering any electrostatic divergences.

Within a "real space" approach, one can solve the eigenvalue problem using a finite element or finite difference approach [9, 12]. We use a higher order finite difference approach owing to its simplicity in implementation. The Laplacian operator can be expressed using

$$\left(\frac{\partial^2\psi}{\partial x^2}\right)_{x_0} \approx \sum_{n=-N}^{N} C_n\, \psi(x_0+nh,y,z) \qquad (6)$$

where h is the grid spacing, N is the number of nearest grid points, and C_n are the coefficients for evaluating the required derivatives [13]. The error scales as $O(h^{2N+2})$.

Once the secular equation is created, the eigenvalue problem can be solved using iterative methods [11, 14]. Typically, a method such as a preconditioned Davidson method can be used. This is a robust and efficient method, which never requires one to store the Hamiltonian matrix. In this paper we outline a method that avoids solving large eigenvalue problems explicitly [11]. The method utilizes a damped *Chebyshev polynomial filtered subspace iteration*. In our approach, only the initial iteration requires solving an eigenvalue problem, which can be handled by means of any available efficient eigensolver. This step is used to provide a good initial subspace (or good initial approximation to the wave functions). Because the subspace dimension is slightly larger than the number of wanted eigenvalues, the method does not require as much memory as standard restarted eigensolvers such as ARPACK and TRLan (Thick - Restart, Lanczos) [15, 16]. Moreover, the cost of orthogonalization is much reduced as the filtering approach only requires a subspace with dimension slightly larger than the number of occupied states and orthogonalization is performed only once per SCF iteration. In contrast, standard eigensolvers using restart usually require a subspace twice as large and the orthogonalization and other costs related to updating the eigenvectors are much higher.

The main idea of the proposed method is to start with a good initial eigen-basis, $\{\psi_n\}$, corresponding to occupied states of the initial Hamiltonian, and then to improve adaptively the subspace by polynomial filtering. That is, at a given self-consistent step, a polynomial filter, $P_m(t)$, of order m is constructed for the current Hamiltonian $\mathscr{H}$. As the eigen-basis is updated, the polynomial will be different at each SCF step since $\mathscr{H}$ will change. The goal of the filter is to make the subspace spanned by $\{\hat{\psi}_n\} = P_m(\mathscr{H})\{\psi_n\}$ approximate the eigen subspace corresponding to the occupied states of $\mathscr{H}$. There is no need to make the new subspace, $\{\hat{\psi}_n\}$, approximate the wanted eigen subspace of $\mathscr{H}$ to high accuracy at intermediate steps. Instead, the filtering is designed so that the new subspace obtained at each self-consistent iteration step will progressively approximate the wanted eigen space of the final Hamiltonian when self-consistency is reached.

This can be efficiently achieved by exploiting the Chebyshev polynomials, C_m, for the polynomials P_m. Specifically, we wish to exploit the fast growth property outside of the [-1, 1] interval. All that is required to obtain a good filter at a given SCF step, is to provide a lower bound and an upper bound of an interval of the spectrum of the current Hamiltonian $\mathscr{H}$. The lower bound can be readily obtained from the Ritz values computed from the previous step, and the upper bound can be inexpensively

This article is copyrighted as indicated in the article. Reuse of AIP content is subject to the terms at: http://scitation.aip.org/termsconditions. Downloaded to IP: 128.83.205.78 On: Fri, 20 Mar 2015 15:45:07

obtained by a very small number of (*e.g.*, 4 or 5) Lanczos steps [11]. Hence the main cost of the filtering at each iteration is in computing the polynomial operation.

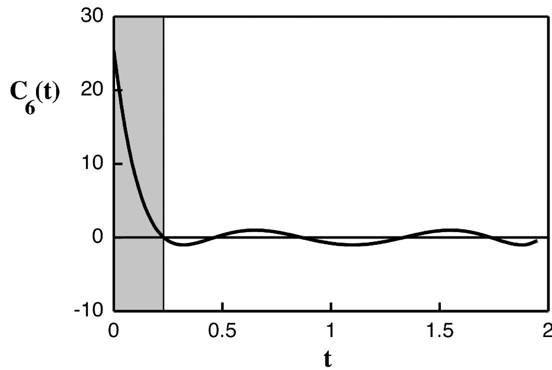

FIGURE 1. Example of a damped Chebyshev polynomial, C_6, the shaded area corresponds to eigenvalue spectrum regime that will be enhanced by the filtering operation (see text).

To construct a "damped" Chebyshev polynomial on the interval [a,b] to the interval [-1,1], one can use an affine mapping such that

$$l(t) = \frac{t-(a+b)/2}{(b-a)/2} \quad (7)$$

The interval is chosen to encompass the energy interval containing the eigen space of interest, *i.e.*, the lowest to highest eigenvalues. The filtering operation can then be expressed as

$$\{\hat{\psi}_n\} = C_m(l(\mathscr{H}))\{\psi_n\} \quad (8)$$

This computation is accomplished by exploiting the convenient three-term recurrence property of Chebyshev polynomials:

$$C_0(t) = 1 \qquad C_1(t) = t$$
$$C_{m+1}(t) = 2t\,C_m(t) - C_{m-1}(t) \quad (9)$$

An example of a damped Chebyshev polynomial as defined by Eqs. 7 and 9 is given in Fig. 1 where we have taken the lower bound as a=0 and the upper bound as b=2. In this example, the filtering would enhance the eigenvalue components in the shaded region.

The filtering procedure for the self-consistent cycle is illustrated in Fig. 2. Unlike traditional methods, the cycle only requires one explicit diagonalization step. Instead of repeating this step again within the self-consistent loop, a filtering operation is used to create a new basis in which the desired eigen subspace is enhanced. After the new basis, $\{\hat{\psi}_n\}$, is formed, the basis is orthogonalized. The orthogonalization step scales as the cube of the number of occupied states and as such this method is not an "order-n" method. However, the prefactor is sufficiently small

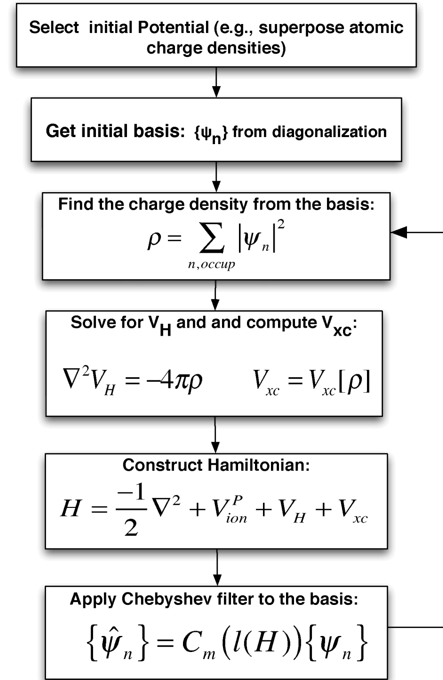

FIGURE 2. Schematic of the self-consistent cycle using Chebyshev filtering.

that the method is much faster than previous implementations of real space methods [11]. The cycle is repeated until the "input" and "output" density is unchanged.

This algorithm allows to examine much larger systems than previously accessible owing to the efficacy of the Chebyshev filtering. Often the code will run more than an order of magnitude faster [11, 17]. In many cases it is now possible to consider nanostructures that span from the "atomic" limit to the "bulk limit".

The Electronic Properties of Si Nanocrystals

We will illustrate the Chebyshev filtering method for a prototypical system: hydrogenated silicon nanocrystals. These nanocrystals, or quantum dots, are small fragments of the bulk in which the surface has been passivated by hydrogen atoms. In the case of silicon, the passivation is accomplished experimentally by capping the surface dangling bonds with hydrogen atoms [3]. These systems exhibit interesting changes as one approaches the nano-regime. For example, nanocrystals of silicon are expected to be optically active, whereas bulk crystals of silicon are not [3, 18].

This article is copyrighted as indicated in the article. Reuse of AIP content is subject to the terms at: http://scitation.aip.org/termsconditions. Downloaded to IP: 128.83.205.78 On: Fri, 20 Mar 2015 15:45:07

The largest dot we examined contained over ten thousand atoms: $Si_{9041}H_{1860}$. This dot is approximately 7 nm in diameter. A ball and stick model for a much smaller quantum dot, approximately, 3 nm in diameter, is illustrated in Fig. 3.

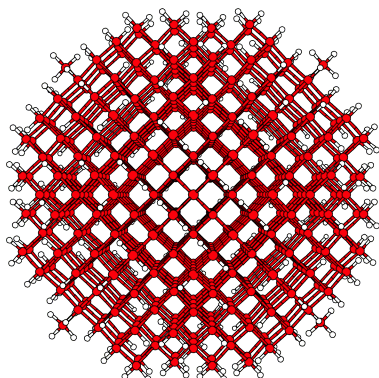

FIGURE 3. Ball and stick model of a hydrogenated silicon quantum dot. The interior consists of a diamond fragment. The surface of the fragment is capped with hydrogen atoms.

A solution of the Kohn-Sham Eq. 1 yields the energy levels or eigenstates for the quantum dot. If the dot is sufficiently large, this spectrum should approach the density of states of crystalline silicon. This is illustrated in Fig. 4. The bulk density of states will reflect van Hove singularities in the energy band topology, *i.e.* , singularities associated with critical points when $\nabla_{\vec{k}} E(\vec{k})$ vanishes

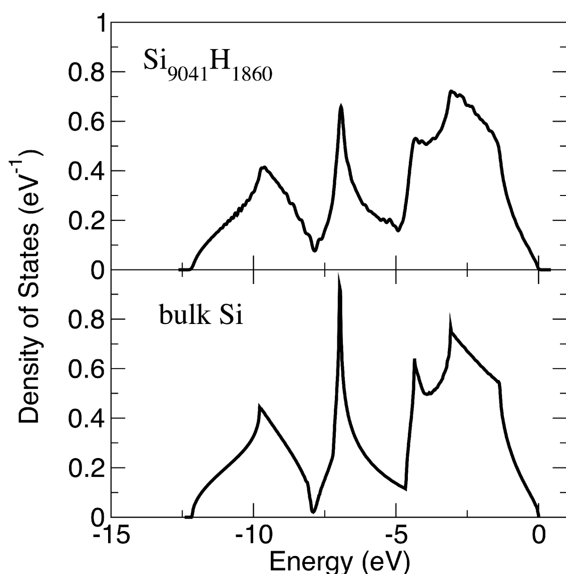

FIGURE 4. Eigenvalue spectrum for a large quantum dot of silicon: $Si_{9041}H_{1860}$ (top panel) compared to the density of states of crystalline silicon (bottom panel). The energy zero is taken to be the highest occupied level for the dot and the valence band maximum for the crystal.

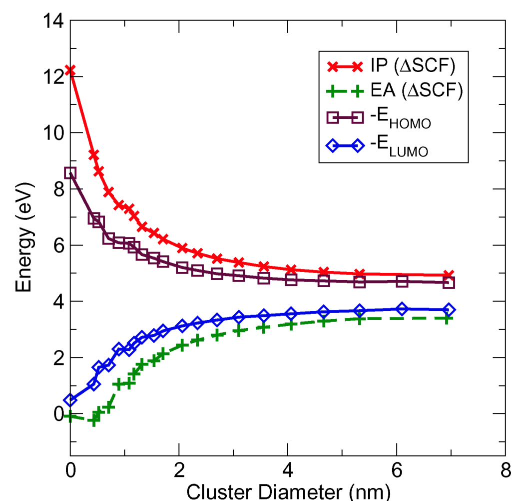

FIGURE 5. Evolution of the ionization potential (IP) and electron affinity (EA) with quantum dot size. Also shown are the eigenvalue levels for the highest occupied molecular orbital (HOMO) and the lowest unoccupied molecular orbital (LUMO).

(where $E(\vec{k})$ is the energy band as a function of the wave vector [19]). The generally good agreement between the density of states for the dot and crystal suggests that by $\sim$7 nm the dot is of sufficient size to capture the van Hove singularities. (The comparison will not be exact because the quantum dot contains Si-H bonds in addition to the Si-Si bonds. In the dot eigenvalue spectrum, this results in the extra contributions near 5 eV.)

We can also examine the evolution of the ionization potentials (I) and the electron affinities (A) for the quantum dot:

$$\begin{aligned} I &= E(N-1) - E(N) \\ A &= E(N) - E(N+1) \end{aligned} \tag{10}$$

The difference between the ionization potential and the electron affinity can be associated with the quasi-particle gap: E_{qp}=I-A. If the exciton (electron-hole) interaction is small, this gap can be compared to the optical gap. However, for silicon quantum dots the exciton energy is believed to be on the order of $\sim$1 eV for dots less than $\sim$1 nm.

We can examine the scaling of the ionization potential and electron affinity by assuming a simple scaling and fitting to the calculated values (shown in Fig. 5):

$$\begin{aligned} I(D) &= I_\infty + A/D^\alpha \\ A(D) &= A_\infty + B/D^\beta \end{aligned} \tag{11}$$

where D is the dot diameter. A fit of these quantities results in I_∞=4.5 eV, A_∞=3.9 eV, α=1.1 and β=1.08. The fit gives a quasi-particle gap of $E_{qp}(D \to \infty) =$

This article is copyrighted as indicated in the article. Reuse of AIP content is subject to the terms at: http://scitation.aip.org/termsconditions. Downloaded to IP: 128.83.205.78 On: Fri, 20 Mar 2015 15:45:07

$I_\infty - A_\infty$=0.6 eV in the limit of an infinitely large dot. This value is in good agreement with the gap found for crystalline silicon using the local density approximation [20]. The gap is not in good agreement with experiment owing to the failure of the local density approximation to describe excited states.

A key aspect of our study is that we can examine the scaling of the ionization potential and electron affinity for quantum dots ranging from silane (SiH_4) to dots with thousand of atoms. We not only verify the limiting value of the quasi-particle gap, we can ascertain how this limit is reached, *i.e.*, how the ionization potential and electron affinity scale with the size of the dot and what the relationship is between these quantities and the highest occupied and lowest empty energy levels.

Doping Si Nanocrystals with P

Electronic and optical properties of semiconductor nanostructures are strongly affected by quantum confinement owing to the reduced dimensionality of these systems [21]. In nanocrystals or quantum dots, where the motion of electrons (or holes) is limited in all three spatial coordinates, quantum confinement results in a strong increase of the optical excitation energies when compared to the bulk [22, 18]. One expects that other electronic and optical properties will be affected as well.

For example, in bulk semiconductors, shallow donors (or acceptors) are crucial in determining the transport properties required to construct electronic devices. Experimental studies of shallow impurities in quantum dots, such as P in Si nanocrystals, have been hampered by difficulties in the preparation of samples in a controllable manner; it is hard to ensure that a quantum dot contains only one impurity. As such, only a few experimental studies have focused on doping of quantum dots. These studies have utilized photoluminescence and electron spin resonance measurements. Increasing the dopant concentration results in distinct changes in its photoluminescence properties such as suppression of the signal [23] and a blue-shift of photoluminescence maxima with decreasing particle size in heavily *p*-doped porous silicon [24]. From these measurements, it is not clear whether or not the doping of Si nanocrystals provides a generation of free charge carriers [24, 25]. Electron spin resonance involves measuring the hyperfine splitting (HFS) of the defect electron levels, which is directly related to localization of the dopant electron density on the impurity site [26]. In Si nanocrystals with radii of 10 nm doped with P, a hyperfine splitting of 110 G has been observed [27]. This splitting is in sharp contrast to the bulk value of 42 G [27]. However, the intensity of the signal was very small compared to the conduction electron signal. A size dependence of the HFS was also found for Si quantum dots with radii around 50 nm [28], although in this case it was probably influenced by an asymmetrical shape of Si crystallites. Recently, a strong size dependence of the HFS of P atoms was observed in much smaller nanocrystallites with radii of 2 - 3 nm [29].

Theoretical studies of shallow impurities in quantum dots have also lagged relative to calculations for pure, undoped systems. The large number of atoms and low symmetry have hindered such studies. Most of the early studies of these systems relied on empirical studies for impurities in quantum dots [30, 31, 32]. These calculations involve the utilization of various parameters, which are usually assumed to have bulk-like values. Another common drawback in these past studies is the use of a generic hydrogen-like potential to model the impurity atom. Recently, some first principles studies have been performed [33, 34], but these studies have been limited to systems with less than 500 atoms.

In contrast to supercell approaches, the real space method outlined earlier allows us to consider energy differences between charged clusters in a straightforward manner [35]. We calculated ionization energies I_d for P-doped nanocrystals and affinity energies A_p for pure Si nanocrystals using charged systems:

$$\begin{aligned} I_d &= E(n-1) - E(n), \\ A_p &= E(n) - E(n+1), \end{aligned} \tag{12}$$

where E is the ground state total energies of the $n-$, $(n+1)-$ and $(n-1)-$electron systems. Our results as a function of nanocrystal's radius are shown in Fig. 7. It is a surprising that the ionization energy I_d shows virtually no dependence on the size of the nanocrystal. It assumes the bulk value of approximately 4 eV even for nanoscale systems.

The binding energy E_B for the donor atom can be calculated as a difference between these two quantities:

$$E_B = I_d - A_p \tag{13}$$

This definition of the binding energy E_B corresponds to two separate processes: First, the doped dot is ionized, *i.e.* the electron is physically removed from the nanocrystal and I_d is determined. Then, it is added to a dot of equivalent size without an impurity atom being present, and A_p is calculated. A similar approach was utilized in tight-binding calculations [32]. This definition of the binding energy for the donor atom can be contrasted with that for a bulk system, where the binding energy is defined as the difference between the dopant electron level and conduction band continuum. In nanocrystals or quantum dots, such a definition is problematic since an electron being excited into an unoccupied state (below the vacuum level) will be confined by the physical size

This article is copyrighted as indicated in the article. Reuse of AIP content is subject to the terms at: http://scitation.aip.org/termsconditions. Downloaded to IP: 128.83.205.78 On: Fri, 20 Mar 2015 15:45:07

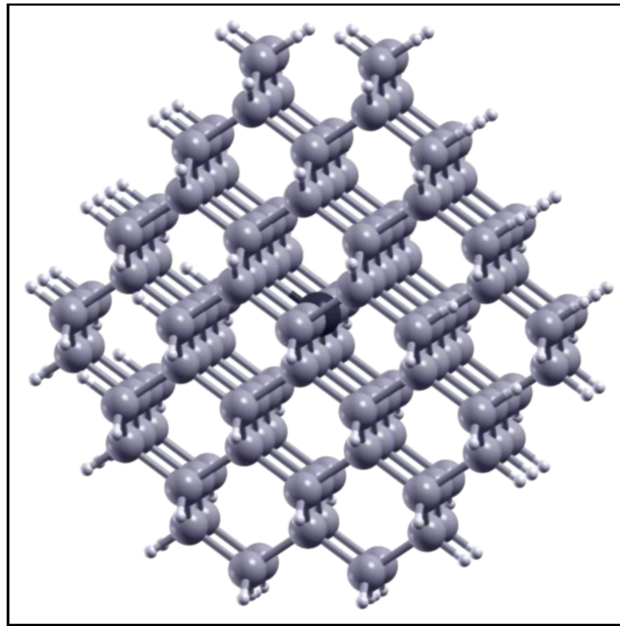

FIGURE 6. Model of P in a Si nanocrystal passivated by H on the surface. The Si atom at the center of the nanocrystal is substituted by P.

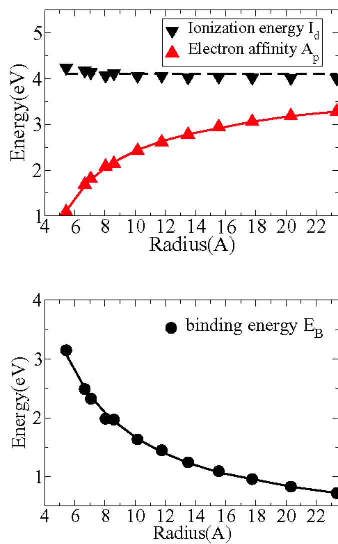

FIGURE 7. Ionization energy I_d, electron affinity A_p, and binding energy E_B of the P electron(as defined in Eq. 12 and 13) in a Si nanocrystal as a function of radius R

of the dot and will continue to interact strongly with the impurity atom.

Also in Fig. 7, the binding energy associated with the donor electron is plotted as a function of the nanocrystal radius up to ∼2.3 nm. If we define a shallow donor to have a binding energy of less than ∼100 meV, then P is not a shallow donor for any of the nanocrystals. One can make a rough extrapolation and see that P will not be shallow for nanocrystals of less than about 50 nm.

The nature of the Si-P bond can be clarified by examining the charge density of the dopant electron $|\Psi(r)|^2$ for several dot sizes. In Fig. 8, we illustrate the charge profile for the case when the impurity is at the dot center. The density is plotted along [100] direction; results in other directions are similar. At all dots radii, the dopant wave function is strongly localized around the impurity site, *i.e.*, the majority of the charge is within the P-Si bond length. From effective mass calculations [36, 37], it follows that the envelope wave function of the dopant electron is given by $j_0(\pi r/R) \propto \sin(\pi r/R)/r$. Our calculated charge profile (Fig. 8) is at variance with this description. This difference in the spatial distributions can be attributed to the weaker screening in quantum dots. At these sizes, the dielectric constant is several times smaller than the bulk value [18, 38], giving rise to the increase of the effective electron-impurity potential and stronger localization of the electron around the defect atom.

Given the charge distribution of the dopant electron, one can evaluate the isotropic hyperfine parameter and the corresponding hyperfine splitting (HFS), which determines the contact interaction between the electron and defect nuclei. We utilized the method of Van de Walle and Blöchl [39] to extract the isotropic hyperfine parame-

This article is copyrighted as indicated in the article. Reuse of AIP content is subject to the terms at: http://scitation.aip.org/termsconditions. Downloaded to IP: 128.83.205.78 On: Fri, 20 Mar 2015 15:45:07

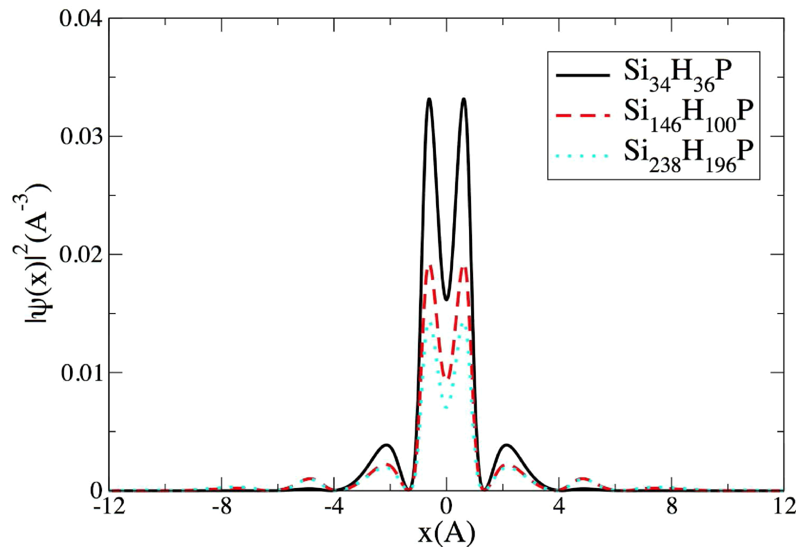

FIGURE 8. Charge density for the dopant electron along the [100] direction for three P-doped Si nanocrystals of different size.

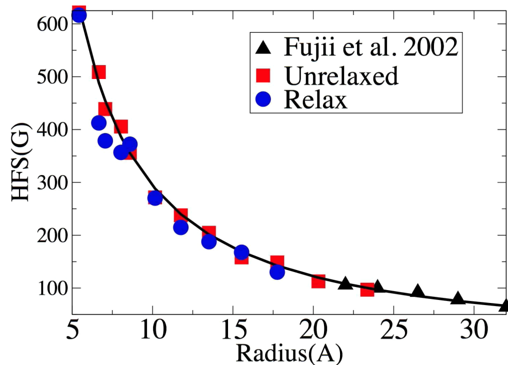

FIGURE 9. Calculated (square and circle) and experimental (triangle) HFS versus the radius R of the P-doped Si nanocrystal. The experimental data is taken from Ref. [29]

ter and the resulting HFS. Our calculated hyperfine splittings for a P atom positioned in the dot center are given in Fig. 9. We also show the results where the Si host is fully relaxed around the P site and where it is not. The results are not very different for the large nanocrystals.

At small nanocrystal sizes, the HFS is very large owing to strong localization of the electron around impurity. As the radius increases, the value of the splitting decreases. Our calculated results scale with radius R of the dot as $R^{-1.5}$ (effective mass theory gives R^{-3}). In Fig. 9, we also present the experimental data [29]. The measured values of the HFS falls on the best fit to calculated results. In our earlier work [33], we were unable to compare to the experimental regime because of the computational load. In this work, our largest nanocrystal has a larger radius than the smallest experimental nanocrystal observed.

We also studied cases in which the P atom substitutes Si atoms in the nanocrystal other than the center one. We found that for Si nanocrystal with radius larger than $\sim$8Å, it is the most energetically favorable for P atom to substitute Si at the dot center. Near the surface, the P atom electron density becomes more delocalized and the HFS shows a notable decrease in the value compared to P at the center position. Neglecting the surface site and the outer layers, the HFS is calculated to vary by only $\sim$10% over the interior sites.

CONCLUSIONS

In summary, we have illustrated a new algorithm for computing the electronic properties of nanostructures and applied this algorithm to properties of hydrogenated Si quantum dots doped with a single phosphorus atom. We calculated the ionization energy and binding energy of the defect. The ionization energy does not exhibit behavior characteristic of quantum confinement; the defect ionization energy remains constant throughout the

This article is copyrighted as indicated in the article. Reuse of AIP content is subject to the terms at: http://scitation.aip.org/termsconditions. Downloaded to IP: 128.83.205.78 On: Fri, 20 Mar 2015 15:45:07

range of sizes studied and equal to the ionization energy of bulk silicon. The charge density associated with the excess dopant electron shows a strong localization towards the impurity site in small dots, and it starts to delocalize when the radius increases. This may be attributed to weak screening in quantum dots resulting in the strong electron-impurity interaction. From our calculated charge density, we evaluated the isotropic hyperfine parameter and HFS for our phosphorus-doped nanocrystals. We found that this quantity is large in small systems and decreases with size, in close agreement with recent experimental findings.

ACKNOWLEDGMENTS

This work was supported in part by the National Science Foundation under DMR-0551195 and the US Department of Energy under DE-FG02-06ER15760 and DE-FG02-06ER46286 . Calculations were performed at the Texas Advanced Computing Center (TACC) and at the National Energy Research Scientific Computing Center (NERSC).

REFERENCES

1. A. P. Alivisatos, *Science* **271**, 933 (1996).
2. M. C. Troparevsky, L. Kronik, and J. R. Chelikowsky, *J. Chem. Phys.* **119**, 2284 (2003).
3. S. Furukawa, and T. Miyasato, *Phys. Rev. B* **38**, 5726 (1988).
4. I. Vasiliev, S. Öğüt, and J. R. Chelikowsky, *Phys. Rev. B* **65**, 115416 (2002).
5. W. Kohn, and L. J. Sham, *Phys. Rev.* **140**, A1133 (1965).
6. J. R. Chelikowsky, and M. L. Cohen, "Pseudopotentials for Semiconductors," in *Handbook of Semiconductors*, edited by T. S. Moss, and P. T. Landsberg, Elsevier, Amsterdam, 1992.
7. G. Kresse, and J. Furthmüller, *Phys. Rev. B* **54**, 11169 (1996).
8. J. R. Chelikowsky, N. Troullier, and Y. Saad, *Phys. Rev. Lett.* **72**, 1240 (1994).
9. T. Torsti, T. Eirola, J. Enkovaara, T. Hakala, P. Havu, V. Havu, T. Höynälänmaa, J. Ignatius, M. Lyly, I. Makkonen, T. T. Rantala, J. Ruokolainen, K. Ruotsalainen, E. Räsänen, H. Saarikoski, and M. J. Puska, *phys. stat. solidi* **243**, 1016 (2006).
10. L. Kronik, A. Makmal, M. L. Tiago, M. M. G. Alemany, M. Jain, X. Huang, Y. Saad, and J. Chelikowsky, *phys. stat. sol. (b)* **243**, 1063 (2006).
11. Y. Zhou, Y. Saad, M. L. Tiago, and J. R. Chelikowsky:, *J. Comp. Phys.* **219**, 172 (2006).
12. T. L. Beck, *Rev. Mod. Phys.* **72**, 1041 (2000).
13. B. Fornberg, and D. M. Sloan, *Acta Numerica* **94**, 203 (1994).
14. A. Stathopoulos, S. Öğüt, Y. Saad, J. Chelikowsky, and H. Kim, *Comput. Sci. Eng.* **2**, 19 (2000).
15. R. B. Lehoucq, D. C. Sorensen, and C. Yang, *ARPACK Users Guide: Solution of Large Scale Eigenvalue Problems by Implicitly Restarted Arnoldi Methods*, SIAM, Philadelphia, 1998, URL `http://www.caam.rice.edu/software/ARPAC`.
16. K. Wu, A. Canning, H. D. Simon, and L. W. Wang, *J. Comp. Phys.* **154**, 156 (1999).
17. J. R. Chelikowsky, M. L. Tiago, Y. Saad, and Y. Zhou, *Comp. Phys. Commun.* (in press).
18. S. Ogut, and J. R. Chelikowsky, *Phys. Rev. B* **55**, R4914 (1997).
19. J. R. Chelikowsky, and M. L. Cohen, *Phys. Rev. B* **14**, 556 (1976).
20. L. J. Sham, and M. Schlüter, *Phys. Rev. Lett.* **51**, 1888 (1983).
21. A. D. Yoffe, *Adv. Phys.* **50**, 1 (2001).
22. I. Vasiliev, J. R. Chelikowsky, and R. M. Martin, *Phys. Rev. B* **65**, 121302 (2002).
23. A. Mimura, M. Fujii, S. Hayashi, D. Kovalev, and F. Koch, *Phys. Rev. B* **62**, 12625 (2000).
24. G. Mauckner, W. Rebitzer, K. Thonke, and R. Sauer, *Solid State Comm.* **91**, 717 (1994).
25. D. Kovalev, H. Heckler, G. Polisski, and F. Koch, *Phys. Status Solidi B* **215**, 871 (1999).
26. G. Feher, *Phys. Rev.* **114**, 1219 (1959).
27. J. Müller, F. Finger, R. Carius, and H. Wagner, *Phys. Rev. B* **60**, 11666 (1999).
28. B. J. Pawlak, T. Gregorkiewicz, C. A. J. Ammerlaan, and P. F. A. Alkemade, *Phys. Rev. B* **64**, 115308 (2001).
29. M. Fujii, A. Mimura, S. Hayashhi, Y. Yamamoto, and K. Murakami, *Phys. Rev. Lett.* **89**, 206805 (2002).
30. C. Y. Fong, H. Zhong, B. M. Klein, and J. S. Nelson, *Phys. Rev. B* **49**, 7466 (1994).
31. I. H. Lee, K. H. Ahn, Y. H. Kim, R. M. Martin, and J. P. Leburton, *Phys. Rev. B* **60**, 13720 (1999).
32. M. Lannoo, C. Delerue, and G. Allan, *Phys. Rev. Lett.* **74**, 3415 (1995).
33. D. Melnikov, and J. R. Chelikowsky, *Phys. Rev. Lett.* **92**, 046802 (2004).
34. Z. Zhou, M. L. Steigerwald, R. A. Friesner, L. Brus, and M. S. Hybertsen, *Phys. Rev. B* **71**, 245308 (2005).
35. J. R. Chelikowsky, *J. Phys. D: Appl. Phys.* **33**, R33 (2000).
36. L. E. Brus, *J. Chem. Phys.* **79**, 4403 (1983).
37. L. E. Brus, *J. Chem. Phys.* **80**, 5566 (1983).
38. S. Öğüt, R. Burdick, Y. Saad, and J. R. Chelikowsky, *Phys. Rev. Lett.* **90**, 127401 (2003).
39. C. G. V. de Walle, and P. E. Blöchl, *Phys. Rev. B* **47**, 4244 (1993).

This article is copyrighted as indicated in the article. Reuse of AIP content is subject to the terms at: http://scitation.aip.org/termsconditions. Downloaded to IP: 128.83.205.78 On: Fri, 20 Mar 2015 15:45:07